Nucleate pool boiling heat transfer on etched and laser structured silicon surfaces

Anže Sitar[a,*], Matic Može[a], Michele Crivellari[b], Jörg Schille[c], Iztok Golobič[a]

[a]University of Ljubljana, Faculty of Mechanical Engineering, Aškerčeva 6, 1000 Ljubljana, Slovenia

[b]Fondazione Bruno Kessler, Center for Materials and Microsystems, Via Sommarive 18, I - 38123 Povo, Trento, Italy

[c]University of Applied Sciences Mittweida, Laser Institute, Technikumplatz 17, 09648 Mittweida, Germany

* Corresponding author:

Phone: +386 1 4771 702;

Fax: +386 1 4771 773;

E-mail: anze.sitar@fs.uni-lj.si.

Abstract

Pool boiling experiments were performed using saturated double-distilled and degassed water on 10 × 10 mm silicon samples, which were (i) untreated; (ii) laser structured; or (iii) modified with etched artificial nucleation cavities. The etched silicon surfaces were fabricated with differently sized micro nucleation cavities (5 - 30 µm) and pitches (0.125 - 2 mm) to allow a comparative analysis of the fabricated surfaces. The heat transfer coefficient (HTC) comparative analysis conducted at the heat flux of 200 kW/m^2 exhibits the highest enhancement of 244 % during nucleate boiling on the silicon sample with etched nucleation cavities with a 30 µm diameter and a 0.125 mm pitch. The experimental results consistently show that HTC increases with decreasing the pitch and increasing the size of the nucleation cavities in the range of the experimental conditions. The superheat required for the onset of nucleate boiling and the critical heat flux were not substantially affected with the structured surfaces. However, the boiling phenomena propagates more promptly to the entire available silicon surface, when the sample is laser treated or etched compared to the reference bare silicon sample.

Keywords: nucleate pool boiling; nucleation cavities; laser structuring; onset of nucleate boiling; heat transfer coefficient; critical heat flux.

Highlights

- The heat transfer coefficient (HTC) is improved with surface structuring.
- The largest manufactured cavities were most successful at increasing the HTC.
- The highest density of nucleation cavities resulted in the highest HTCs.
- The onset of boiling, HTC and critical heat flux were not directly correlated.
- The laser textured surfaces improved the HTC compared to the bare silicon surface.

Nomenclature

A	area, m^2
g	gravitational acceleration, m/s^2
h	heat transfer coefficient, W/m^2K
h_{lv}	latent heat of vaporization, J/kg
k	thermal conductivity, W/mIK
q	heat flux, W/m^2
r	radius, m
R	thermal resistance, K/W
T	temperature, °C
w	relative measurement uncertainty, -
x	thickness, m
δ	thermal boundary layer, m
ΔT	temperature difference, K
Δx	distance, m
$\Delta\rho$	density difference, kg/m^3
θ	contact angle, rad
λ	length, m
ρ	density, kg/m^3
σ	surface tension, N/m

Subscripts

0,1,2,3…	consecutive numbering
ave	average
bulk	bulk

c	capillary, cavity
Cu	copper
max	maximum
min	minimum
r	receding
R1	at thermal resistance R_1
R2	at thermal resistance R_2
sat	saturated
Si	silicon
v	vapor
w	wall

Superscripts

’	at the bottom
”	at the top

1. Introduction

In the latter years, we are witnessing an incredibly fast development of new electronic devices and components, which become smaller and more powerful with every iteration of the development process. This miniaturization also brings new challenges in terms of cooling since the performance of classic methods such as forced convection using air and finned surfaces is being pushed to the limit. Hence, new methods are being researched and readied for the application of cooling various electronic devices. The most prominent method is the application of phase-change heat transfer for cooling purposes, as boiling can be used very effectively to reduce the temperatures of the cooled components. A widely studied and used example of phase-change process is pool boiling, which is much simpler to utilize than flow boiling since no artificial circulation is required. An important drawback of cooling via boiling is a rather ineffective heat transfer on very smooth surfaces such as untreated silicon. Therefore, boiling heat transfer needs to be improved for safe and efficient operation of various components, which requires the development of enhanced surfaces.

A great number of publications dealing with surfaces for enhanced boiling heat transfer appeared in the past decade. Some of the notable achievements are presented in the following paragraphs. Udaya Kumar et al. [1] modified the surface of copper samples using plasma-enhanced chemical vapor deposition (PECVD) of graphene and carbon nanotubes, which enhanced the heat transfer coefficient (HTC) and the critical heat flux (CHF) during boiling of FC-72 for up to 155 % and 40 %, respectively. Gouda et al. [2] micromachined interrupted and uninterrupted channels onto copper, which severely enhanced the boiling heat transfer. Hong et al. [3] coated a copper surface with Cu_2O cubic crystals and dendritic structures, which significantly reduced the superheat required for the onset of nucleate boiling (ONB) and enhanced the HTC at low superheats. Jo et al. [4, 5] used supersonic nozzles to coat surfaces with either copper particles or silver nanorods achieving a notable improvement of the boiling heat transfer. Lay et al. [6] fabricated porous graphene structures on copper which allowed ultrafast permeation of water and enhanced the HTC for 151 %. Lee et al. [7] produced a nanorod forest on the surface using metal-assisted chemical etching, which significantly improved the CHF. Wang et al. [8] noted a great increase of the HTC on a porous copper surface, manufactured by hydrogen bubble template deposition method. Zupančič et al. [9] laser textured stainless steel foils to fabricate preferential nucleation sites which significantly enhanced the boiling heat transfer and made the spatial temperature distribution more uniform.

In a follow-up study [10], they compared the performance of laser-textured surfaces in boiling of water and FC-72. Rahman et al. [11] fabricated a superbiphilic surface using highly porous nickel-coated tobacco mosaic virus in combination with a hydrophobic polymer coating and reported HTC in excess of 100 kW/m^2K. Može et al. [12] used laser texturing to significantly enhance both the HTC and the CHF on copper surfaces by fabrication of microcavities serving as preferential nucleation sites.

While many methods focus on copper, which is one of the most common materials in heat transfer engineering due to its excellent thermal conductivity, silicon is equally if not more important especially in microelectronic applications where immersion cooling can take place directly on the silicon-made components. Therefore, application of surface enhancement techniques to silicon is extremely important. Betz et al. [13, 14] created biphilic surfaces on silicon by combining etched or untreated hydrophilic silicon with PTFE-coated hydrophobic islands. The authors recorded extreme improvements of the HTC, especially at low heat fluxes. Yu et al. [15] tested the pool boiling performance of artificial microcavities on silicon surfaces using FC-72. They found that a higher density of artificial cavities results in higher HTC enhancement at high heat fluxes but reduced the value of the CHF. The larger cavities proved to be unfavorable in the scope of heat transfer. Yao et al. [16] grew copper and silicon nanowires on a silicon substrate and found that these (super)hydrophilic structures enhance the CHF by a factor of up to three, whereas the CHF on the reference bare silicon sample was found to be 674 kW/m^2. Similar study was also published by Chen et al. [17] with a measured CHF of 820 kW/m^2 on a bare silicon sample. Pratik et al. [18] applied a foam-like hierarchical hexagonal boron nitride nanomaterial to silicon surfaces and tested them in pool boiling of water in vertical orientation. They demonstrated higher HTCs at moderate and high heat flux relative to bare silicon but a comparable CHF value. Cao et al. [19] fabricated pin-fin structures on silicon surfaces followed by pool boiling tests using FC-72, where they demonstrated that in comparison to the smooth surface, boiling heat transfer and the CHF were significantly enhanced by the pin-fin surfaces and the maximum superheat was considerably decreased. Seo et al. [20] reported an increase of HTC as well as CHF on silicon surfaces by etching relatively large millimeter scale holes into the silicon boiling surface of 32 × 32 mm. The improved boiling heat transfer is attributed to an additional water supply to the hole patterned silicon samples. The CHF value of 802 kW/m^2 was reported for the reference silicon sample. The relations between ONB, HTC and CHF during pool boiling on modified silicon surfaces are

presented by Liu et al. [21]. The CHF on the reference silicon sample was measured in three runs with an average value of 1020 kW/m^2. The authors are explaining the detrimental effect of early nucleation on the CHF with an impairment of wettability at high heat fluxes due to the frequent bubble departure, which increases the liquid flow resistance to the dried out sections of the heated surface. The published CHF results on bare untreated silicon surfaces have a large scatter, which was the initiative for the present experimental study.

The motivation for the presented study was to perform a comparative experimental analysis of water boiling on variously structured silicon surfaces with an aim to transfer the results and conclusions to flow boiling in silicon microchannels. Thus, we have limited the fabrication technologies to etching and laser structuring, as both can be applied with the same operating procedure also to microchannels. Although, the pool boiling process differs from the flow boiling phenomena in the scope of bubble nucleation, growth and departure, we are interested in acquiring an insight to improving the boiling surfaces based on solid experimental results. The final adaptation of the surface structuring for flow boiling applications will be performed after additional experimental work on flow boiling heat transfer.

2. Experiment and theoretical background

2.1 Experimental setup and procedure

The experimental setup was comprised of the pool boiling chamber presented in Fig. 1 which was connected to measurement and supplemental equipment which included: variable transformers for supplying heating power for the immersion and cartridge heaters; data acquisition unit Agilent 34972A with a multiplexer card 34902A; and a personal computer. The boiling chamber has double glazed glass walls to lower the heat losses, an immersion heater to increase the working fluid's temperature to the saturation point, the test section, and additional components to assure the construction stability, alignment, no leakage, and thermal insulation. Additional details of the experimental setup are given in Može et al. [12].

The pool boiling test section is presented in Fig. 2 and comprised of: a copper block with cartridge heaters and thermocouples, a copper disc with a thermocouple, a silicon sample, aerogel insulation and a PEEK holder. In order to reduce the contact thermal resistance a thin layer of thermal paste with a thermal conductivity of 8.5 W/mK was deposited between the silicon sample, the copper disc and the copper block. There was no possibility of adding a thermocouple into the silicon sample due to its small thickness, which was countered by assuring the two interfacial thermal resistances R_1 and R_2 between copper block, coper disc and the silicon sample are as similar as possible. This assembly allows an approximation of the unknown and unmeasurable thermal resistance R_2, as we are able to derive the thermal resistance R_1 with the measured temperatures T_0 and T_1 and calculated heat flux via utilizing the Fourier's law. The lateral heat losses are regarded as negligible, therefore one-dimensional heat conduction is considered in the copper block to derive the heat flux. The layer of an adhesive with a low thermal conductivity of 1 W/mK was deposited on top of the copper disc to hinder boiling from the copper surface, which was needed as the copper disc has a diameter of 18 mm, whereas the silicon sample boiling area is 10 × 10 mm.

The boiling vessel is open to the atmospheric conditions through a small opening port to ensure no pressure increase in the vessel occurs during boiling at higher heat fluxes. An additional consequence of the open vessel is the fluctuation of the water saturation temperature, since it is pressure dependent. The atmospheric pressure was fluctuating during the measurement period from 958 mbar to 1004 mbar and the corresponding saturation temperatures were ranging from 98.45 °C to 99.75 °C in accordance with the equation acquired in [22]. The working fluid in all

of the performed experiments was double distilled water, which was degassed by vigorous boiling with the immersion heaters for two hours. Afterwards, the degassed water was cooled down to approximately 80 °C to exclude any potential trapped vapor embryos on the silicon surface. The cartridge heaters were used to gradually heat up the copper block, copper disc and the silicon sample, whereas the immersion heaters were used to increase the water temperature and maintain the saturated state. The data acquisition unit was programmed to measure all of the temperatures with a frequency of 1 Hz. The progressively increasing heat flux was eventually high enough to initiate the ONB, and the heat flux was further increased and at a certain point decreased to acquire the saturated pool boiling curve. Some experiments were carried out to monitor the ONB, and others to measure the CHF or the HTC. The heat flux was gradually increased and decreased to monitor quasi-steady states of the saturated water pool boiling. The reference silicon samples were untreated with the initial RMS roughness of 0.65 nm, whereas additional samples were prepared with etching potential nucleation cavities with a diameter 5-30 μm and laser structuring with a surface RMS roughness from 646 nm to 2788 nm.

2.2 Silicon surface morphology and nucleation criteria

The produced silicon samples are listed in Table 1; all of them originate from the same reference silicon material, which was afterwards laser structured with three different operating conditions, or etched to fabricate artificial cavities with various diameters and pitches, or tested without any additional surface treatment. The silicon samples are labeled in accordance with the surface morphology in the subsequent paragraphs and chapters.

The silicon samples 10 × 10 mm with a 0.625 mm thickness were mounted on top of a copper disc with an 18 mm diameter, as presented in Fig. 3 (a). The adhesive layer was added to hinder boiling on the copper surface, therefore to compensate for the size mismatch between the copper disc and the silicon samples. The reference untreated sample is given in Fig. 3 (b), whereas the samples with the etched artificial nucleation cavities at different pitches 125-2000 μm are seen in Fig. 3 (c-f). The etched area of the 10 × 10 mm samples is 64 mm^2. A scanning electron microscope (SEM) image of the silicon sample with cavities of 10 μm in diameter at a 125 μm pitch is given in Fig. 3 (g). The optimal pitch for the pool boiling heat transfer is reported by Rahman et al. [23] on copper substrates and Voglar et al. [24] on stainless steel foils to be the capillary length defined by

$$\lambda_c = \sqrt{\frac{\sigma}{g\Delta\rho}} \,. \qquad (1)$$

Surface tension is denoted with σ, the liquid-vapor density difference is $\Delta\rho$, and g is the gravitational acceleration. The optimal pitch increased the HTC as well as CHF during saturated nucleate pool boiling due to the optimized bubble dynamics [23]. The simulation results presented by Gong and Cheng [25] are depicting an inhibition of bubble nucleation at small pitch between the nucleation sites. Furthermore, a simulation revealed the highest boiling heat transfer at pitches of approximately 2.25 and 4.5 times larger than the capillary length for the hydrophilic and hydrophobic rough surfaces, respectively. Ma et al. [26] further investigated the effect of the nucleation site pitch and concluded there is little to no effect in the nucleate boiling regime, however the pitch had a substantial effect on the CHF. The simulations included two pitches of pillars with hydrophobic tips with a factor of 0.45 and 1.41 multiplied by approximately the capillary length. The material of the sample does not affect the capillary length, as it is only a function of the working fluid's properties, therefore the boiling surface material should not affect the optimal pitch. In our experimental work we have been using saturated water at atmospheric pressure, which corresponds to the capillary length of 2.5 mm.

The etched artificial nucleation sites were 50 μm deep with the diameters ranging from 5 μm to 30 μm, as it is presented by SEM photographs in Fig. 4 (a-d). The smallest cavities were not entirely cylindrical, as the features in the micron range are difficult to produce accurately with etching technologies. The initial substrate was a 625 μm thick single-side polished silicon wafer with the crystal orientation of (100). The silicon samples were etched by utilizing the Deep Reactive Ion Etching (DRIE) process in an Alcatel AMS200 plasma etcher at the Micro-Nano Facility of the Fondazione Bruno Kessler (Trento, Italy). The sizes of the etched artificial nucleation cavities were determined in accordance with: (i) the fabrication possibilities; (ii) nucleation criteria; and (iii) our previous experimental experience. The pitch of the nucleation sites was established on the basis of similar published experimental studies [23, 24].

The three different laser treatments of the silicon surface resulted in the topographies presented in Fig. 5 (a-c). An ultrashort pulse laser system with a wavelength of 1030 nm was employed to structure the silicon surface by multiple overlapping parallel passes. The laser structuring parameters (hatch distance, scan speed, spatial pulse distance, laser power, number of scan passes…) have been varied to produce three different surface topologies with the average

feature heights of 3 µm, 9 µm, and 14 µm denoted with laser_1-3. The RMS surface roughness for the laser_1-3 treatments were 646 nm, 1514 nm, and 2788 nm, respectively. The presented topographies show that the most cavities exist on the laser_2 sample in Fig. 5 (b), whereas the most distinctive pillars are present on the laser_3 surface Fig. 5 (c). The potential nucleation cavities are depicted with a blue color, whereas the pillars are red in the topography images.

The optimal radii of surface cavities for them to serve as preferential active nucleation sites can be estimated theoretically using the so-called nucleation criteria. One of the most well-known is Hsu's nucleation criterion [27] which considers a gas/vapor filled cavity on the heated surface, surrounded by saturated liquid. Kandlikar et al. [28] published a similar criterion, which takes into account the contact angle and can account for the subcooling of the liquid

$$\left\{r_{c,\min}, r_{c,\max}\right\} = \frac{\delta \sin\theta_r}{2.2}\left(\frac{T_w - T_{sat}}{T_w - T_{bulk}}\right)\left(1 \mp \sqrt{1 - \frac{8\sigma T_{sat}\left(T_w - T_{bulk}\right)}{\rho_v h_{lv}\delta\left(T_w - T_{sat}\right)^2}}\right). \qquad (2)$$

In the Eq. 3, θ_r denote the receding contact angle; σ the surface tension; T_{sat} the saturation temperature; h_{lv} the latent heat of vaporization; ρ_v the density of vapor; δ the thickness of the thermal boundary layer; T_{bulk} the temperature of the bulk liquid; and T_{w} the temperature of the boiling surface. Other nucleation criteria were published by Bergles and Rohsenow [29], Davis and Anderson [30], and Liu et al. [31]. Fig. 6 shows a comparison of the nucleation criteria for saturated pool boiling of water at atmospheric pressure with the thickness of the thermal boundary layer fixed at 340 µm and the static and receding contact angles of water on the silicon surface 60° and 50°, respectively. According to nucleation criteria the boiling will take place at lower wall superheats in larger nucleation cavities with diameters ranging up to 200 µm. Most of the nucleation criteria predict the lowest temperature of the ONB on the silicon samples with the largest etched nucleation sites, which had a radius of 15 µm. The sizes of the nucleation sites produced with the laser treatment are difficult to assess, as a threshold for a cavity size and shape would be required, therefore only the etched cavities are graphically depicted in Fig. 6. The silicon samples were etched to manufacture nucleation cavities of specific sizes and pitches, however the vast majority of the sample was not treated, therefore the wettability of the etched samples were generally the same as the reference sample. The laser structured surface becomes superhydrophilic compared to the initial hydrophilic reference surface, due to the formation of SiO_2 [32].

2.3 Data reduction

The thermal conductivity of the copper block is a very influential parameter, as the heat flux is acquired indirectly from the temperature measurements. Thus, we made a curve fitting using linear regression from the experimental data on thermal conductivity of copper found in the literature [33]. The equation is defined with

$$k_{Cu} = -1.91 \cdot 10^{-5} T_{ave}^{2} - 5.03 \cdot 10^{-2} T_{ave} + 416 , \qquad (3)$$

in which the T_{ave} is the arithmetic mean of the two nearest measured temperatures in degrees K, whereas the thermal conductivity k_{Cu} is calculated in units W/mK. There are four temperature sensors T_1-T_4 located in the axis of the copper block, and the heat flux is identical at any cross section between the measured temperatures due to negligible lateral heat losses. Therefore, the actual distances between the locations of the temperature sensors were slightly adjusted to compensate for the errors in positioning and the accuracy of the thermocouples in the copper block. The compensations of the distances are given in Table 2, whereas the boiling curves during an experiment on the sample Si_30_1000 with the original and the compensated distances are given in Figure 7 (a) and (b), respectively.

The compensations of the distances between the measured locations yielded a substantial equalization of the corresponding heat fluxes, which differed due to the positioning errors and measurement uncertainty. The heat flux $q_{1\text{-}4}$ was used in all of the subsequent calculations and analysis, as it is the most accurate value, due to the largest distance between the measurement locations. The heat flux in the copper block was calculated from the measured temperatures and the compensated distance as

$$q_{1-4} = k_{Cu,1-4} \frac{\Delta T_{1-4}}{\Delta x_{1-4}} . \qquad (4)$$

The average thermal conductivity of the copper block $k_{Cu,1\text{-}4}$ was calculated by using Eq. 4 and the arithmetic mean of the temperatures T_1 and T_4. The cross section of the copper block A_{Cu} and the silicon samples A_{Si} are different, however the heat transfer rate remains unaltered, if the heat losses are negligible. Therefore, the wall heat flux was calculated as

$$q_w = \frac{A_{Cu}}{A_{Si}} q_{1-4} . \qquad (5)$$

The contact thermal resistance R_1 located between the copper disc and the copper block was calculated from the measured temperatures as

$$R_1 = \frac{T'_{R1} - T''_{R1}}{q_{1-4} A_{Cu}} . \quad (6)$$

The temperatures at the bottom T'_{R1} and the top T''_{R1} of the gap between the copper disc and the copper block were calculated in accordance with the Fourier law and the measured temperatures T_0 and T_1. The thermal resistance of the gap between the copper disc and the silicon sample R_2 was not possible to derive from the temperature measurements, as the silicon sample is not equipped with a thermocouple. Thus, the thermal resistance R_2 was estimated to be 0.1 K/W for all of the measurements, which was the average value calculated for the thermal resistance R_1, based on the temperature measurements. The temperature of the wall was calculated from the equation

$$T_w = T''_{R2} - \frac{q_w x_{Si}}{k_{Si}} , \quad (7)$$

in which the x_{Si} is the thickness of the silicon sample with a value of 625 μm, k_{Si} is the thermal conductivity of the silicon and T''_{R2} is the top temperature of the R_2 gap. The silicon thermal conductivity was iteratively calculated in accordance with the equation valid from 423 °C to 873 °C [22]. The temperature at the top T''_{R2} and at the bottom T'_{R2} of the gap between the copper disc and the silicon sample were calculated as

$$T''_{R2} = T'_{R2} - q_{1-4} A_{Cu} R_2 \quad (8)$$

and

$$T'_{R2} = T_0 - \frac{q_{1-4} \Delta x_{R2-0}}{k_{R2-0}} . \quad (9)$$

The distance Δx_{R2-0} is the distance between the R_2 gap and the location of the thermocouple T_0 and is equal to 1.5 mm. The thermal conductivity of the copper disc between the thermocouple T_0 and the gap R_2 was iteratively calculated in accordance with the Eq. 4 at the arithmetic mean of the temperatures T'_{R2} and T_0. The wall superheat is defined with the equation

$$\Delta T = T_w - T_{bulk} . \quad (10)$$

The heat transfer coefficient is according to the Newton's law of cooling defined as

$$h = \frac{q_w}{\Delta T}. \tag{11}$$

2.4 Measurement uncertainty

The relative measurement uncertainty of the wall heat flux was derived from the equation

$$w\left(q_w\right) = \sqrt{w^2\left(A_{Cu}\right) + w^2\left(A_{Si}\right) + w^2\left(q_{1-4}\right)}, \tag{12}$$

in which the uncertainty of the copper block heat flux is defined with

$$w\left(q_{1-4}\right) = \sqrt{w^2\left(k_{Cu,1-4}\right) + w^2\left(T_1\right) + w^2\left(T_4\right) + w^2\left(\Delta x_{1-4}\right)}. \tag{13}$$

The relative measurement uncertainty is extremely high at low heat fluxes, due to the small temperature differences, and lowers to approximately 4 % at the wall heat flux of 200 kW/m^2. The wall superheat measurement uncertainty was derived from the equation

$$w\left(\Delta T\right) = \sqrt{w^2\left(T_w\right) + w^2\left(T_{bulk}\right)}. \tag{14}$$

The bulk temperature measurement uncertainty was straightforwardly calculated to a value of 1.5 %, as it depends only on the used measurement equipment. The wall temperature measurement uncertainty is more complex with several influential parameters included in it's the definition

$$T_w = T_0 - q_{1-4}\left(\frac{R_2\Delta x_{R2-0} + k_{R2-0}A_{Cu}}{R_2 k_{R2-0}}\right) - \frac{q_w x_{Si}}{k_{Si}}. \tag{15}$$

The wall temperature relative measurement uncertainty is decreasing with increasing wall heat flux and equals to 7.5 % at 200 kW/m^2. The HTC measurement uncertainty is a function of both aforementioned uncertainties, and it therefore also heat flux dependent. The relative HTC measurement uncertainty is equal to 8.5 % at the wall heat flux of 200 kW/m^2.

3. Results and discussion

3.1 Thermal simulation and visualization

The boiling experiments were carried out on 10 × 10 mm silicon samples, which were positioned on a copper disc with a diameter of 18 mm. In order to suppress boiling from the exposed copper area, which was not covered by the silicon sample, we added a layer of adhesive with low thermal conductivity of 1 W/mK. Furthermore, we conducted a thermal simulation of the anticipated temperature field of the test section. The simulation was performed in the SOLIDWORKS environment with a bonded component contact with no local thermal resistance. Although, the simulation is simplified to a large extent, it provides a good estimation for the temperature differences at the top of the test section, which was the motive for the simulation. Our goal was to use an adhesive with an adequately low thermal conductivity to lower the temperature on the top of the adhesive substantially compared to the top of the silicon sample. The performed simulation revealed an 11 K temperature difference between the average temperatures of the top of the silicon sample compared to the top of the adhesive. The thermal simulation was performed to avoid ambiguous experimental results which would occur, if the boiling phenomena would be present at the top of the silicon sample as well as at the top of the adhesive layer. The numerical calculations revealed a substantial temperature difference between the silicon and the adhesive and we concluded that bubbles will not nucleate at the adhesive layer during the nucleate boiling regime, as the temperatures of the adhesive were sufficiently decreased. The detail of the thermal simulation is seen in Fig. 8, which reveals an average temperature of the top of the silicon sample 120 °C and the average temperature of the top of the adhesive 109 °C. The numerical results were acquired at simplified boundary conditions: the surrounding air temperature 25 °C, the heat transfer coefficient to the surrounding air 10 W/m^{2}K, the boiling heat transfer coefficient 3000 W/m^{2}K, and the heater temperature 125 °C.

The conformation of the performed numerical analysis is possible only with a boiling experiment. The synchronized visualization and measurement data acquisition of a boiling experiment on a silicon sample Si_20_0125 are presented in Fig. 9. The presented images and the corresponding states on the boiling curve are undoubtedly confirming that the boiling of water occurred solely on the silicon sample, whilst no bubbles nucleated on the adhesive layer due to the lower temperature and lack of suitable nucleation sites. The onset of boiling occurred

at approximately 10 K of superheat as seen in Fig. 9 (a) with two bubble towers emerging from the etched nucleation sites. The heat flux was increased and the majority of the silicon surface became boiling active, as seen in Fig. 9 (b). Afterwards, the heat flux was gradually decreased and the visualized states presented in Fig. 9 (c-g) are depicting the lowering of the bubble nucleation activity on the silicon sample with the boiling end presented in Fig. 9 (h). All of the visualized states of the test section clearly show that there is no boiling occurring at the top of the adhesive layer, which is crucial for the comparative analysis of the various samples used.

3.2 Boiling curves and heat transfer coefficient with comparative analysis

We believe that the next step in modifying the silicon surfaces is the implementation of laser texturing, as it offers the possibility of inexpensive fabrication of microsized features to promote early onset of boiling and heat transfer enhancement during nucleate boiling. Recently, Kruse et al. [34] published the improvement of HTC as well as CHF by implementing laser structures on stainless steel. We have manufactured three different surfaces denoted with Si_laser_1-3 with differently sized surface features. The boiling curves acquired on the laser structures samples and the reference silicon sample are presented in Fig. 10. The ONB was recorded at wall superheats ranging from 7 K to 17 K. The boiling curves are clearly showing enhanced heat transfer on the laser structured samples Si_laser_1 and Si_laser_2 with a lower superheat of approximately 5 K at the heat flux of 300 kW/m^2. The boiling curves acquired on sample Si_laser_3 are depicting slightly enhanced heat transfer, however the experimental results show an improvement below expectations. The laser structuring procedure for the boiling surface was determined on ad hoc basis in these experiments and needs optimization in the direction of improving the number and size of the cavities, which were the lacking feature on the surface Si_laser_3.

The boiling curves acquired from the experiments performed on the reference smooth silicon sample and the silicon samples with 5 µm diameter holes with pitches from 0.125 to 2 millimeters are presented in Fig. 11. The results are exhibiting that the HTC is enhanced with increasing the number of artificial nucleation sites with lowering the pitch between the etched 5 µm nucleation cavities. The boiling curves show that the nucleation sites with the 2 mm spacing were not beneficial in the scope of the heat transfer, as there is little-to-no difference compared to the reference silicon sample. On the other hand, the nucleation cavities with the pitches of 0.125 mm and 0.5 mm had a very similar effect on the boiling curve, as the superheat

was lowered for approximately 7 K at 300 kW/m^2 compared to the reference. The superheat required for the ONB ranged from 11 K to 15 K for all the silicon samples, however a large difference between the tested samples is seen in the boiling curves themselves, as almost the entire surface became boiling active shortly after the ONB on the samples Si_5_0125 and Si_5_0500. On the other hand, samples Si_5_1000, Si_5_2000 and Si_ref were gradually increasing the active boiling surface area, which is seen as a large difference between the wall superheat during the increasing and decreasing heat flux.

The effect of the etched nucleation cavities with the diameter of 5, 10, 20, and 30 μm at the 0.125 mm pitch is presented in Fig. 12 along with the reference silicon sample. The goal of this side by side comparison is to find the cavity diameter with the largest impact on the nucleate pool boiling heat transfer at the 0.125 mm pitch, which was found as best with the smallest cavities of 5 μm in diameter. Several experimental runs on the same silicon sample were made to evaluate the repeatability of the boiling curves and are denoted with r1-r4. The measurements show good repeatability of the experiment in the scope of the HTC, however the wall superheat required for the boiling incipience differs when comparing different experimental runs on the same silicon sample. Additionally, extensive experimental work resulted in detachment of the silicon sample in the last runs of the samples Si_10_0125, Si_20_0125, and Si_30_0125, which is seen as an uncharacteristic highly superheated wall in excess of 20 K. The comparative analysis of the boiling curves presented in Fig. 12 unambiguously reveals that the largest enhancement of the boiling heat transfer was achieved on the silicon sample with the largest etched cavities with a diameter of 30 μm. The wall superheat difference at the heat flux of 300 W/m^2 between the sample Si_30_0125 and the Si_ref sample is approximately 15 K. The silicon samples with smaller cavities etched at the surface improved the boiling heat transfer performance to a lesser degree. Moreover, the experimental results also consistently show that increasing the nucleation site diameter improved the nucleate boiling phenomena. Some of the boiling curves presented in Fig. 12 were acquired in the nucleate boiling regime all the way to the CHF, which occurred in the region from 450 kW/m^2 to 650 kW/m^2. The structured surfaces exhibit little-to-no effect on the CHF in the range of the prepared samples, which is additionally confirmed in Fig. 13.

Additional experimental work was performed on the samples with 30 μm cavities with variations in the pitches from 0.125 mm to 2 mm, as seen in Fig. 13. The repeatability of the experimental runs is more than adequate, as all of the experimental repetitions on the same silicon sample are exhibiting a very similar HTC. However, the ONB and CHF are varying among subsequent experimental runs on the same sample. The sample Si_30_2000 is showing small to no improvement of the HTC compared to the reference sample, whereas all the other samples with etched 30 μm nucleation sites are depicting an increase in the HTC, which is the highest in the sample Si_30_0125 with the smallest pitch between the artificially fabricated cavities. The wall superheat needed for the ONB ranged from 2 K to 20 K, whereas the CHF was recorded from 500 W/m^2 to 750 W/m^2. The ONB and CHF were not substantially or consistently improved with the performed surface structuring, therefore no conclusions on the influential parameters can be made on the basis of the presented experiments.

The HTC enhancement at three heat fluxes is presented in Fig. 14, whereas the HTC values at the heat flux of 200 kW/m^2 are given in Table 3. The maximum HTCs attained on different silicon samples are compared to the reference sample at the same heat flux to assure that the operating conditions are utterly comparable. The maximum HTC achieved was approximately 50 kW/m^{2}K at heat fluxes exceeding 400 kW/m^2 during boiling on the sample Si_30_0125. The experimental data up to the heat flux of 300 kW/m^2 is presented in Fig. 14. In most cases the HTC is slightly lower during the increasing heat flux segment of the boiling curve, as the boiling phenomenon does not simultaneously occur on the entire area of the silicon sample. Hence, the maximum values of the HTC are taken into consideration to ensure the most comparable operating conditions are obtained. Namely, the progress of the boiling propagation across the entire available surface is rather complex, difficult to control and is prone to variations on the same sample during multiple experimental runs. As it is seen in Fig. 14, the HTC was increased on almost all of the structured samples compared to the reference sample. The laser structured samples slightly increased the HTC, similarly as the samples with the large 2 mm pitch between the etched cavities. The largest increase of the HTC is seen during boiling on the sample Si_30_0125, followed by the samples Si_20_0125 and Si_10_0125. These results indicate that the pitch was the most influential parameter in the scope of HTC improvement. The experimental results are also exhibiting that larger nucleation cavities increased the HTC also at the lowest heat flux of 100 kW/m^2, which is coherent with the nucleation criteria. Namely,

large nucleation sites are expected to be active during boiling at low superheat (low heat flux), whereas smaller nucleation cavities require higher superheat and therefore higher heat flux.

The HTC values at 200 kW/m^2 were compared and the results are gathered in Table 3. Some of the samples were excluded from comparison for clarity. The laser structured silicon samples have a slightly improved HTC, with the maximum enhancement of +31.5 % noted with the sample Si_laser_2. All the samples with the etched nucleation cavities ranging from 5 µm to 30 µm in diameter at a pitch of 125 µm have a significantly improved HTC compared to the values achieved on the reference sample. The enhancements of the HTC at the heat flux of 200 kW/m^2 for the samples with etched nucleation sites were 41.4 % for the smallest 5 µm nucleation cavities and 244.1 % for the largest 30 µm artificial nucleation sites. The experimental results are consistent; the HTC increases with decreasing the pitch and increasing the size of the nucleation cavities in the range of the experimented parameters.

4. Conclusions

Pool boiling experiments were performed in order to allow for a comparative analysis of nucleate boiling heat transfer on silicon surfaces, fabricated using two different methods. Experimental setup and procedure were adequately designed for comparison of the effect of the surface treatments, as: (i) the repeatability of the HTC of the subsequent experimental runs was very good; (ii) boiling was observed solely on the silicon surface; (iii) the effect of nucleation cavities size and pitch on pool boiling heat transfer is consistent.

The silicon samples 10 × 10 mm were either left untreated; laser structured to produce three different surface roughness levels; or etched with the DRIE procedure to fabricate artificial nucleation sites with a diameter of 5 μm, 10 μm, 20 μm, and 30 μm with a pitch of 125 μm, 500 μm, 1000 μm, and 2000 μm. The experimental results consistently exhibit that increasing the nucleation site diameter and decreasing the pitch between the artificial cavities is beneficial in increasing the nucleate boiling HTC. The boiling heat transfer enhancement originates from the increased number of active nucleation sites, which was improved with lowering the pitch as well as with proper sizing of the artificial cavities. The largest improvement of the HTC was observed with the largest nucleation cavities with a diameter of 30 μm and the smallest pitch of 0.125 mm. The presented results were not entirely expected as there are experimental studies of pool boiling on copper and stainless steel available [23, 24], in which the authors have shown the best results of HTC and CHF improvements are achieved with the pitch between the nucleation sites being equal to the capillary length. In our case the capillary length of saturated water at atmospheric conditions is 2.5 mm, therefore the best improvement should be seen at the pitch of 2 mm. We agree that the optimal bubble dynamic requires a certain pitch between the nucleation sites, however the capillary length depends solely on the working fluid, which could be insufficient. The explanation of the contradictory results could be in the material and the surface conditions, as the bubble departure and rewetting is surely dependent on the working fluid's properties as well as the sample material properties and surface conditions. The boiling HTC on laser structured surfaces was improved, however the enhancements on the etched surfaces by far surpassed the heat transfer performance of the laser treated surfaces. The laser treatment produced a surface structure with pronounced pillars, however the boiling heat transfer would be more substantially enhanced by producing high density adequately sized nucleation sites. In addition, the laser treatment also affects the surface wettability, which becomes highly hydrophilic and therefore affects the bubble nucleation, liquid replenishment

and boiling heat transfer. The benefits of the laser structuring remain its versatility, the possibility of micro structuring, and transferability to microchanels. However, additional steps need to be taken towards the optimization of the laser treatment procedure, which would result in a surface with a vastly improved CHF, HTC, and/or ONB compared to bare silicon.

The wall superheat required for the ONB as well as the achieved CHF were not substantially affected by all of the variations in surface structuring done by etching or laser texturing. An important difference between the ONB and the boiling incipience on the entire surface exists, which is manifested as an extended ONB hysteresis. If the entire available surface becomes active in the scope of boiling at the ONB, there is a small or no difference in the boiling curve during increasing or decreasing heat flux after the boiling is initiated. The superheat required for the commencement of nucleate boiling on the reference bare silicon sample is comparable to other samples with surface modifications, however the boiling curves acquired on the reference sample are exhibiting the most extended ONB hysteresis, which indicates the slowest transition to the nucleate boiling regime on the entire available sample surface. Hence, the randomly fabricated nucleation sites on the untreated surface were not adequate to initiate boiling on the entire available surface at a low superheat.

The measured absolute results should be interpreted with caution, as one of the contact thermal resistance was estimated, which has a significant impact on the wall superheat and the HTC. However, the experimental results and following trends are consistent over all of the performed experimental runs, which is attributable to the boiling phenomena and not an outcome of the estimated thermal resistance fluctuation.

5. References

[1] G. Udaya Kumar, K. Soni, S. Suresh, K. Ghosh, M.R. Thansekhar, P. Dinesh Babu, Modified surfaces using seamless graphene/carbon nanotubes based nanostructures for enhancing pool boiling heat transfer, Exp. Therm. Fluid Sci., 96 (2018) 493-506.

[2] R.K. Gouda, M. Pathak, M.K. Khan, Pool boiling heat transfer enhancement with segmented finned microchannels structured surface, Int. J. Heat Mass Transfer, 127 (2018) 39-50.

[3] S. Hong, S. Jiang, Y. Hu, C. Dang, S. Wang, Visualization investigation of the effects of nanocavity structure on pool boiling enhancement, Int. J. Heat Mass Transfer, 136 (2019) 235-245.

[4] H.S. Jo, M.-W. Kim, T.G. Kim, S. An, H.-G. Park, J.-G. Lee, S.C. James, J. Choi, S.S. Yoon, Supersonically spray-coated copper meshes as textured surfaces for pool boiling, Int. J. Therm. Sci., 132 (2018) 26-33.

[5] H.S. Jo, T.G. Kim, J.-G. Lee, M.-W. Kim, H.G. Park, S.C. James, J. Choi, S.S. Yoon, Supersonically sprayed nanotextured surfaces with silver nanowires for enhanced pool boiling, Int. J. Heat Mass Transfer, 123 (2018) 397-406.

[6] K.K. Lay, J.S. Ong, K.Y. Yong, M.K. Tan, Y.M. Hung, Nucleate pool boiling enhancement by ultrafast water permeation in graphene-nanostructure, Int. Commun. Heat Mass, 101 (2019) 26-34.

[7] D. Lee, B.S. Kim, H. Moon, N. Lee, S. Shin, H.H. Cho, Enhanced boiling heat transfer on nanowire-forested surfaces under subcooling conditions, Int. J. Heat Mass Transfer, 120 (2018) 1020-1030.

[8] Y.-Q. Wang, J.-L. Luo, Y. Heng, D.-C. Mo, S.-S. Lyu, Wettability modification to further enhance the pool boiling performance of the micro nano bi-porous copper surface structure, Int. J. Heat Mass Transfer, 119 (2018) 333-342.

[9] M. Zupančič, M. Može, P. Gregorčič, I. Golobič, Nanosecond laser texturing of uniformly and non-uniformly wettable micro structured metal surfaces for enhanced boiling heat transfer, Applied Surface Science, 399(Supplement C) (2017) 480-490.

[10] P. Gregorčič, M. Zupančič, I. Golobič, Scalable Surface Microstructuring by a Fiber Laser for Controlled Nucleate Boiling Performance of High- and Low-Surface-Tension Fluids, Sci. Rep., 8(1) (2018) 7461.

[11] M.M. Rahman, E. Ölçeroğlu, M. McCarthy, Scalable Nanomanufacturing of Virus-templated Coatings for Enhanced Boiling, Advanced Materials Interfaces, 1(2) (2014) 1300107.

[12] M. Može, M. Zupančič, M. Hočevar, I. Golobič, P. Gregorčič, Surface chemistry and morphology transition induced by critical heat flux incipience on laser-textured copper surfaces, Applied Surface Science, 490 (2019) 220-230.
[13] A.R. Betz, J. Xu, H. Qiu, D. Attinger, Do surfaces with mixed hydrophilic and hydrophobic areas enhance pool boiling?, Applied Physics Letters, 97(14) (2010) 141909.
[14] A.R. Betz, J. Jenkins, C.-J.C. Kim, D. Attinger, Boiling heat transfer on superhydrophilic, superhydrophobic, and superbiphilic surfaces, Int. J. Heat Mass Transfer, 57(2) (2013) 733-741.
[15] C.K. Yu, D.C. Lu, T.C. Cheng, Pool boiling heat transfer on artificial micro-cavity surfaces in dielectric fluid FC-72, Journal of Micromechanics and Microengineering, 16(10) (2006) 2092-2099.
[16] Z. Yao, Y.W. Lu, S.G. Kandlikar, Effects of nanowire height on pool boiling performance of water on silicon chips, Int. J. Therm. Sci., 50(11) (2011) 2084-2090.
[17] R. Chen, M.-C. Lu, V. Srinivasan, Z. Wang, H.H. Cho, A. Majumdar, Nanowires for Enhanced Boiling Heat Transfer, Nano Letters, 9(2) (2009) 548-553.
[18] K.C. Pratik, A. Nammari, T.S. Ashton, A.L. Moore, Saturated pool boiling heat transfer from vertically oriented silicon surfaces modified with foam-like hexagonal boron nitride nanomaterials, Int. J. Heat Mass Transfer, 95 (2016) 964-971.
[19] Z. Cao, B. Liu, C. Preger, Z. Wu, Y. Zhang, X. Wang, M.E. Messing, K. Deppert, J. Wei, B. Sundén, Pool boiling heat transfer of FC-72 on pin-fin silicon surfaces with nanoparticle deposition, Int. J. Heat Mass Transfer, 126 (2018) 1019-1033.
[20] H. Seo, Y. Lim, H. Shin, I.C. Bang, Effects of hole patterns on surface temperature distributions in pool boiling, Int. J. Heat Mass Transfer, 120 (2018) 587-596.
[21] Y. Liu, M.-C. Lu, D. Xu, The suppression effect of easy-to-activate nucleation sites on the critical heat flux in pool boiling, Int. J. Therm. Sci., 129 (2018) 231-237.
[22] R. Rowley, W. Wilding, J. Oscarson, N. Giles, DIPPR® Data Compilation of Pure Chemical Properties, Design Institute for Physical Properties, AIChE, USA, 2010.
[23] M.M. Rahman, J. Pollack, M. McCarthy, Increasing Boiling Heat Transfer using Low Conductivity Materials, Sci. Rep., 5 (2015) 13145.
[24] J. Voglar, P. Gregorčič, M. Zupančič, I. Golobič, Boiling performance on surfaces with capillary-length-spaced one- and two-dimensional laser-textured patterns, Int. J. Heat Mass Transfer, 127 (2018) 1188-1196.

[25] S. Gong, P. Cheng, Two-dimensional mesoscale simulations of saturated pool boiling from rough surfaces. Part II: Bubble interactions above multi-cavities, Int. J. Heat Mass Transfer, 100 (2016) 938-948.
[26] X. Ma, P. Cheng, X. Quan, Simulations of saturated boiling heat transfer on bio-inspired two-phase heat sinks by a phase-change lattice Boltzmann method, Int. J. Heat Mass Transfer, 127 (2018) 1013-1024.
[27] Y.Y. Hsu, On the size range of active nucleation cavities on a heating surface, J. Heat Transfer, 84 (1962) 207-216.
[28] S.G. Kandlikar, V.R. Mizo, M.D. Cartwright, E. Ikenze, Bubble nucleation and growth characteristics in subcooled flow boiling of water, in: HTD-Vol. 342, ASME Proceedings of the 32nd National Heat Transfer Conference, 1997, pp. 11-18.
[29] A.E. Bergles, W.M. Rohsenow, The Determination of Forced-Convection Surface-Boiling Heat Transfer, J. Heat Transfer, 86(3) (1964) 365-372.
[30] E.J. Davis, G.H. Anderson, The incipience of nucleate boiling in forced convection flow, AIChE J., 12(4) (1966) 774-780.
[31] D. Liu, P.-S. Lee, S.V. Garimella, Prediction of the onset of nucleate boiling in microchannel flow, Int. J. Heat Mass Transfer, 48(25) (2005) 5134-5149.
[32] C. Yang, X. Jing, F. Wang, K.F. Ehmann, Y. Tian, Z. Pu, Fabrication of controllable wettability of crystalline silicon surfaces by laser surface texturing and silanization, Applied Surface Science, 497 (2019) 143805.
[33] R.W. Powell, P.E. Liley, C.Y. Ho, Thermal conductivity of selected materials, U.S. Dept. of Commerce, National Bureau of Standards; for sale by the Superintendent of Documents, U.S. Govt. Print. Off., Washington, 1966.
[34] C.M. Kruse, T. Anderson, C. Wilson, C. Zuhlke, D. Alexander, G. Gogos, S. Ndao, Enhanced pool-boiling heat transfer and critical heat flux on femtosecond laser processed stainless steel surfaces, Int. J. Heat Mass Transfer, 82 (2015) 109-116.

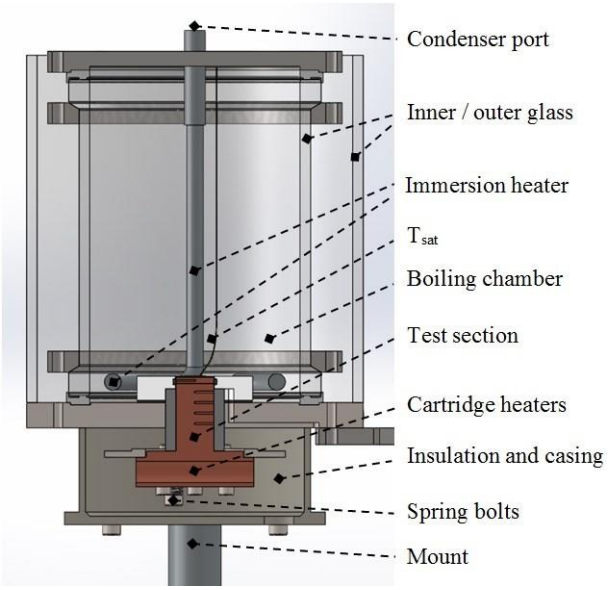

Figure 1. Pool boiling experimental chamber.

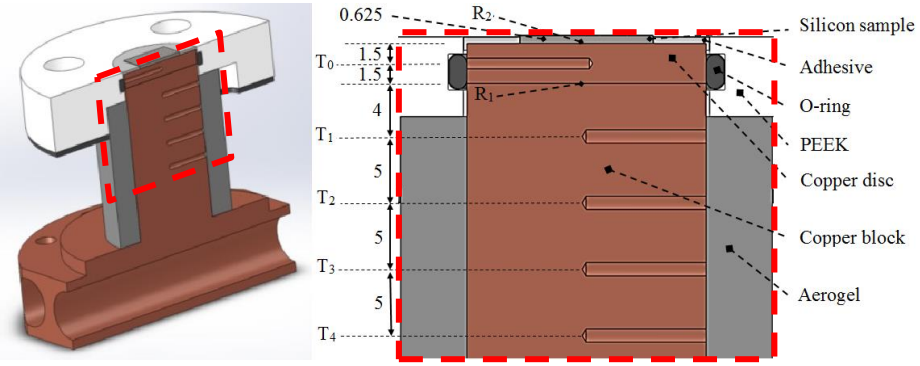

Figure 2. Pool boiling test section.

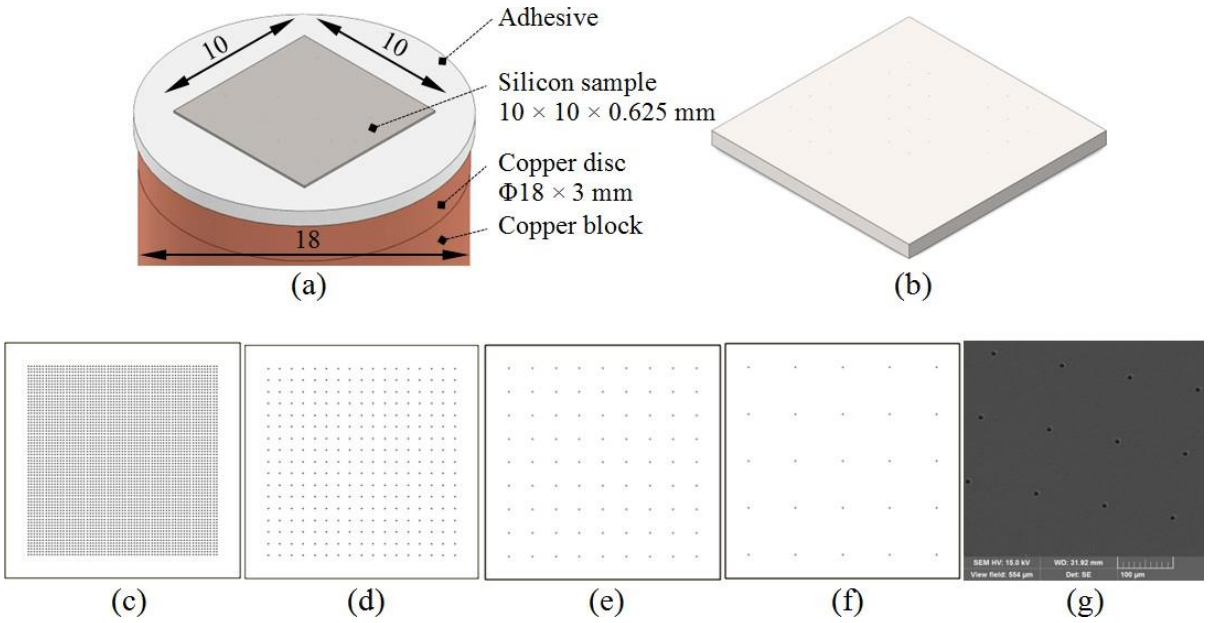

Figure 3. Silicon sample (a) in assembly, (b) untreated reference, (c-f) with etched nucleation cavities at pitches 0.125 mm, 0.5 mm, 1 mm, and 2 mm, (g) SEM of a Si_10_0125 sample.

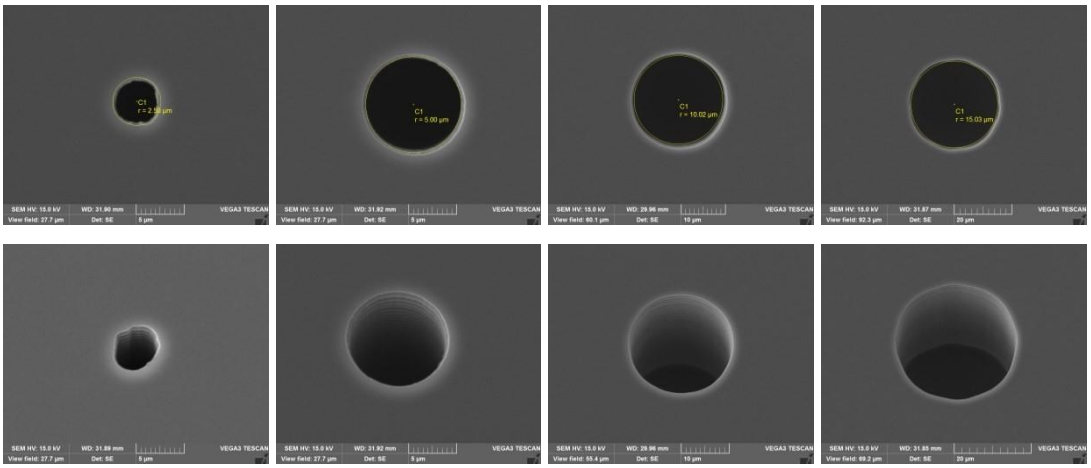

(a) (b) (c) (d)

Figure 4. SEM photographs of the etched nucleation cavities with a diameter of (a) 5 µm; (b) 10 µm; (c) 20 µm; and (d) 30 µm.

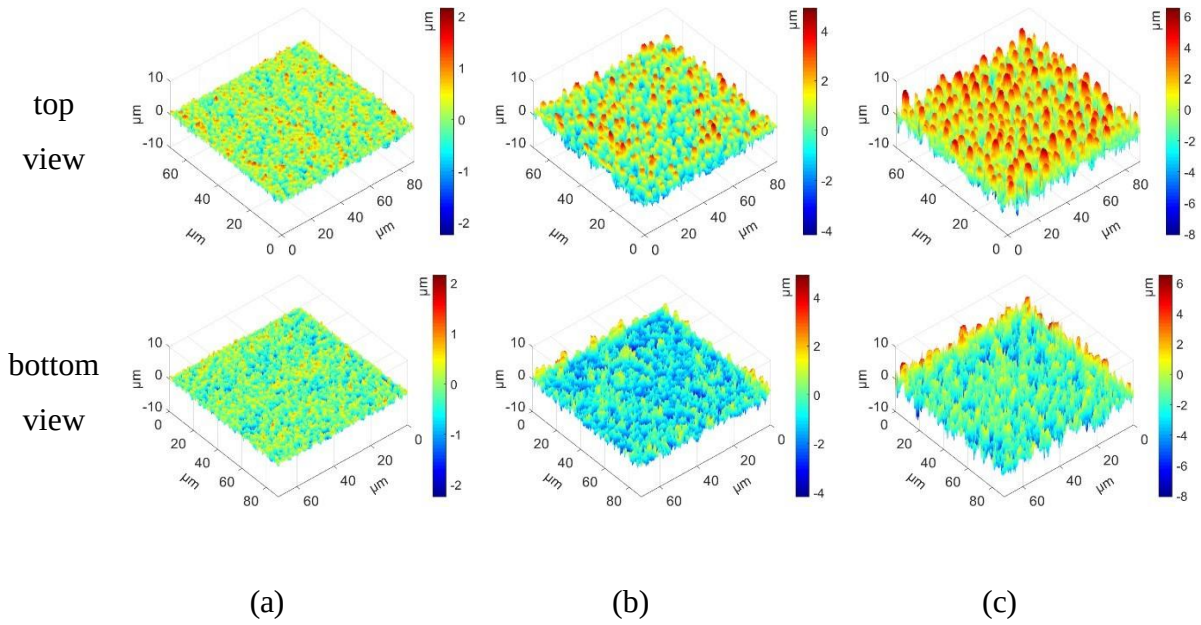

Figure 5. Topographies of the silicon samples with laser structured surface denoted with (a) laser_1, (b) laser_2, and (c) laser_3.

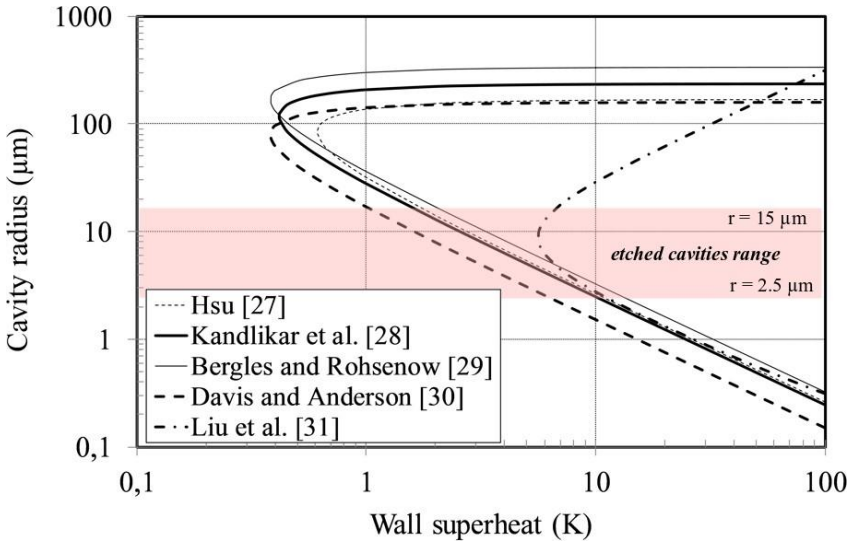

Figure 6. Comparison of nucleation criteria for saturated boiling of water at atmospheric pressure.

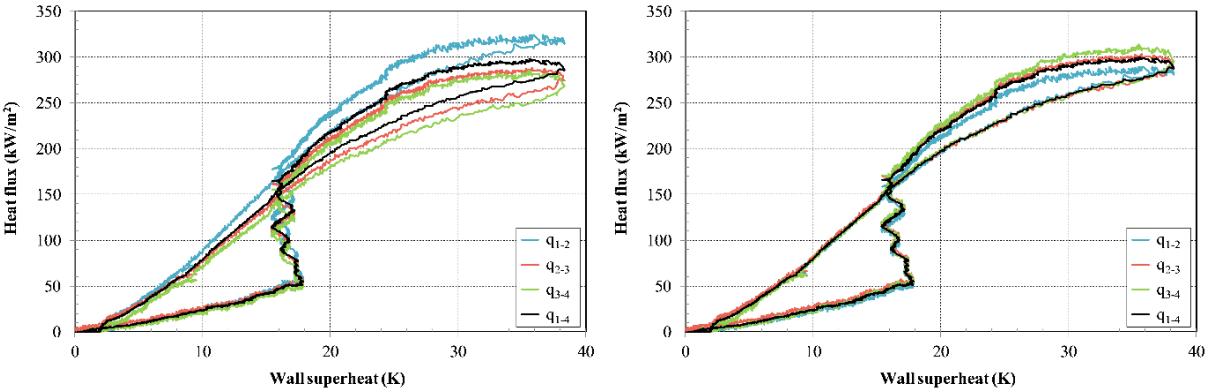

Figure 7. Boiling curves on the sample Si_30_1000_r3 considering all the heat fluxes q_{1-2}, q_{2-3}, q_{3-4}, and q_{1-4} at (a) original design distances, (b) compensated distances.

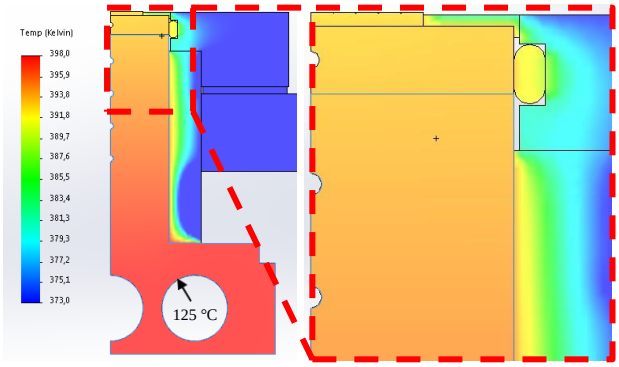

Figure 8. Steady state thermal simulation of the test section.

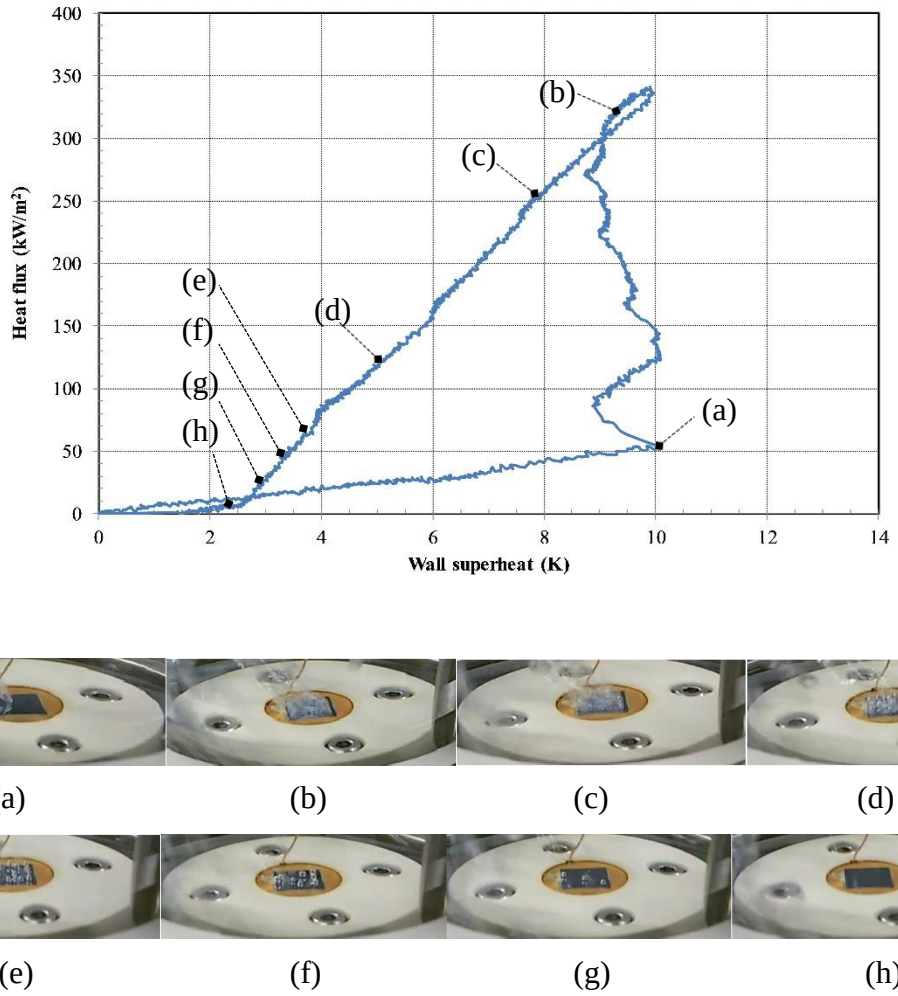

Figure 9. Boiling curve and visualization of boiling on the silicon sample Si_20_0125 with 20 µm cavities at a 0.125 mm spacing (a-h).

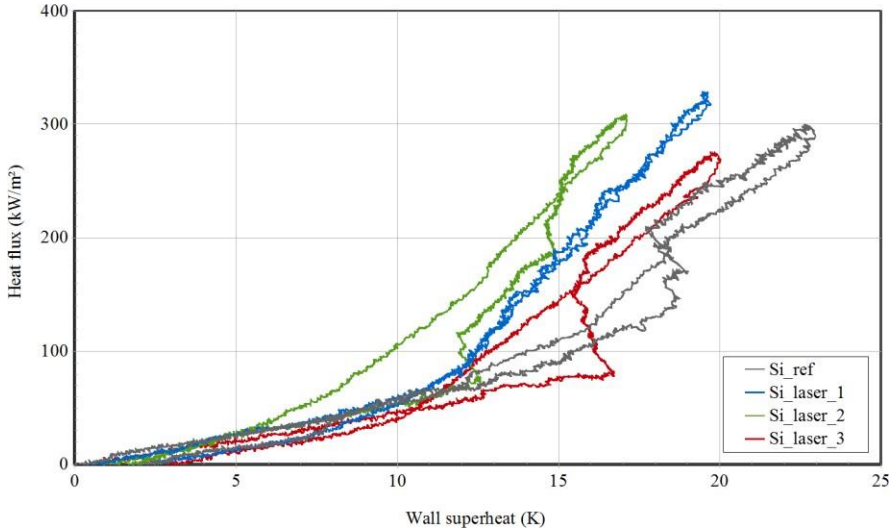

Figure 10. Boiling curves on silicon samples with laser structured surface.

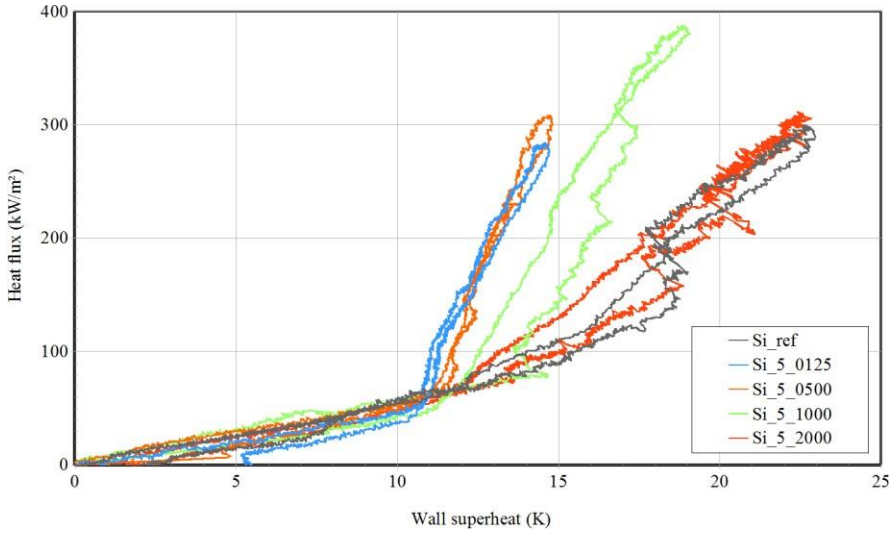

Figure 11. Boiling curves on silicon samples with etched cavities of 5 µm in diameter with pitches from 0.125 to 2 mm.

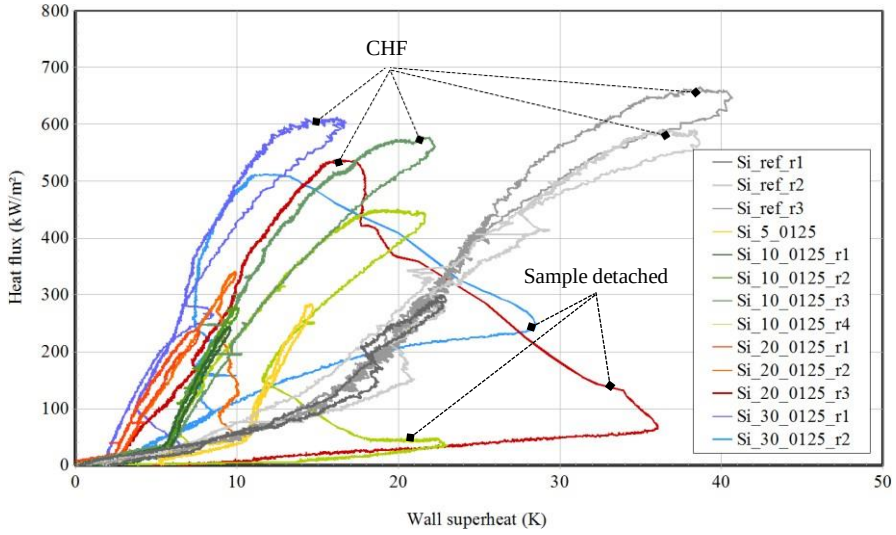

Figure 12. Boiling curves on silicon samples with etched cavities from 5 to 30 microns in diameter.

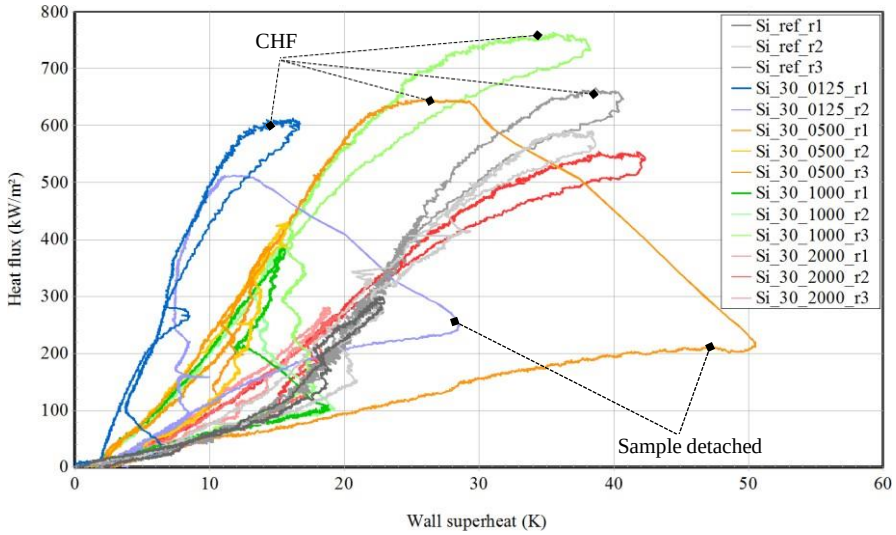

Figure 13. Boiling curves on silicon samples with etched cavities of 30 µm in diameter with pitches from 0.125 to 2 mm.

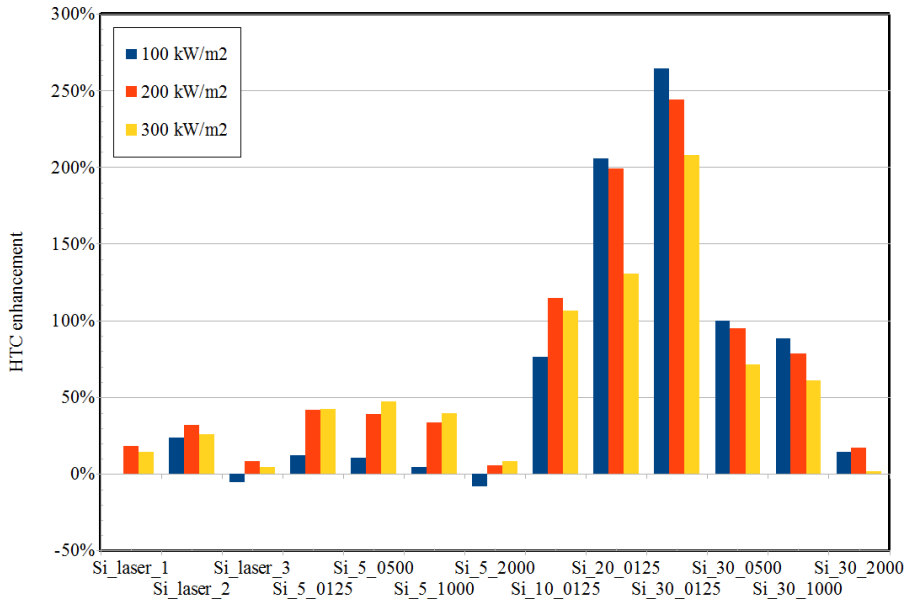

Figure 14. Enhancement of the HTC on etched and laser structured silicon samples.

Table 1. The fabricated silicon samples.

Material	Surface	Label	Cavities diameter (µm)	Cavities pitch (µm)	Surface RMS roughness (nm)
Si	no treatment	ref	no cavities	no cavities	0.65
Si	laser structuring	laser 1, 2, 3	varies	varies	646, 1514, 2788
Si	deep reactive ion etching	diameter / pitch	5, 10, 20, 30	0125, 0500, 1000, 2000	0.65 (outside cavities)

Table 2. The distance between the temperature sensors.

	Δx_{1-2}	Δx_{2-3}	Δx_{3-4}	Δx_{1-4}
original	5 mm	5 mm	5 mm	15 mm
compensated	4.55 mm	4.75 mm	5.6 mm	14.9 mm

Table 3. HTC comparison and achieved enhancements.

Sample label	Surface	HTC at 200 kW/m^2 (kW/m^{2}K)	HTC Enhancement
Si_ref	no treatment	11.1	-
Si_laser_1	laser structuring	13.1	18.0 %
Si_laser_2	laser structuring	14.6	31.5 %
Si_laser_3	laser structuring	12.0	8.1 %
Si_5_0125	deep reactive ion etching	15.7	41.4 %
Si_10_0125	deep reactive ion etching	23.8	114.4 %
Si_20_0125	deep reactive ion etching	33.2	199.1 %
Si_30_0125	deep reactive ion etching	38.2	244.1 %